NANO LETTERS
Cite This: Nano Lett. 2019, 19, 1931−1937
Letter
pubs.acs.org/NanoLett

Anion Exchange and the Quantum-Cutting Energy Threshold in Ytterbium-Doped $CsPb(Cl_{1-x}Br_x)_3$ Perovskite Nanocrystals

Tyler J. Milstein,[†] Kyle T. Kluherz,[†] Daniel M. Kroupa,[†] Christian S. Erickson,[†] James J. De Yoreo,[†,‡] and Daniel R. Gamelin*[,†]

[†]Department of Chemistry, University of Washington, Seattle, Washington 98195-1700, United States
[‡]Physical Sciences Division, Pacific Northwest National Laboratory, Richland, Washington 99352, United States

Supporting Information

ABSTRACT: Colloidal halide perovskite nanocrystals of $CsPbCl_3$ doped with Yb^{3+} have demonstrated remarkably high sensitized photoluminescence quantum yields (PLQYs), approaching 200%, attributed to a picosecond quantum-cutting process in which one photon absorbed by the nanocrystal generates two photons emitted by the Yb^{3+} dopants. This quantum-cutting process is thought to involve a charge-neutral defect cluster within the nanocrystal's internal volume. We demonstrate that Yb^{3+}-doped $CsPbCl_3$ nanocrystals can be converted postsynthetically to Yb^{3+}-doped $CsPb(Cl_{1-x}Br_x)_3$ nanocrystals without compromising the desired high PLQYs. Nanocrystal energy gaps can be tuned continuously from $E_g \approx 3.06$ eV (405 nm) in $CsPbCl_3$ down to $E_g \approx 2.53$ eV (~490 nm) in $CsPb(Cl_{0.25}Br_{0.75})_3$ while retaining a constant PLQY above 100%. Reducing E_g further causes a rapid drop in PLQY, interpreted as reflecting an energy threshold for quantum cutting at approximately twice the energy of the Yb^{3+} $^2F_{7/2} \rightarrow {}^2F_{5/2}$ absorption threshold. These data demonstrate that very high quantum-cutting energy efficiencies can be achieved in Yb^{3+}-doped $CsPb(Cl_{1-x}Br_x)_3$ nanocrystals, offering the possibility to circumvent thermalization losses in conventional solar technologies. The presence of water during anion exchange is found to have a deleterious effect on the Yb^{3+} PLQYs but does not affect the nanocrystal shapes or morphologies, or even reduce the excitonic PLQYs of analogous undoped $CsPb(Cl_{1-x}Br_x)_3$ nanocrystals. These results provide valuable information relevant to the development and application of these unique materials for spectral-shifting solar energy conversion technologies.

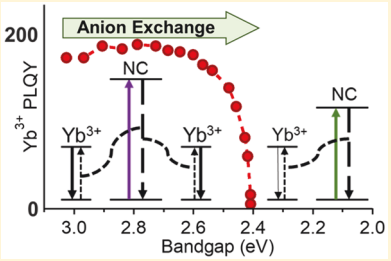

KEYWORDS: *Perovskite nanocrystals, ytterbium doping, anion exchange, quantum cutting*

Nanocrystals (NCs) of the all-inorganic lead-halide perovskite semiconductors, $CsPbX_3$ ($X = Cl^-$, Br^-, I^-), have demonstrated attractive photophysical properties such as band-gap tunability throughout the visible, broad absorption with large absorption cross sections, narrow emission line widths, near-unity photoluminescence quantum yields (PLQYs), and defect tolerance.[1−3] Consequently, these materials have generated intense interest for numerous optoelectronics, photovoltaics, and photodetection applications.[4−7] Impurity doping with cations such as Mn^{2+}, Zn^{2+}, Cd^{2+}, Sn^{2+}, and others has also been explored as an approach to tune these optoelectronic properties.[8−10] Mn^{2+} doping has received particular attention for shifting the NC PL relative to its absorption, and this approach has yielded families of luminescent materials that may be useful for white-light generation or other novel applications.[11−16]

Recently, colloidal Yb^{3+}-doped $CsPb(Cl_{1-x}Br_x)_3$ NCs (Yb^{3+}:$CsPb(Cl_{1-x}Br_x)_3$) were demonstrated to show extraordinarily high PLQYs in the near-IR sensitized by the photoexcitation of the $CsPb(Cl_{1-x}Br_x)_3$ host NC, reaching as high as ~170%.[17−19] These very high PLQYs have been attributed to an extremely efficient quantum-cutting process that converts the energy from one short-wavelength absorbed photon into the energies of multiple longer-wavelength emitted photons. The emissive $^2F_{5/2} \rightarrow {}^2F_{7/2}$ f−f transition of Yb^{3+} in $CsPb(Cl_{1-x}Br_x)_3$, at ~980 nm, is aligned very well with the peak energy-conversion efficiency of crystalline Si (c-Si) photovoltaics, suggesting promise for various solar spectral-conversion applications.[17,20−22] Solar-energy conversion using quantum cutting has been investigated for many years with other lanthanide-containing luminescent materials,[20,21,23−27] but Yb^{3+}:$CsPb(Cl_{1-x}Br_x)_3$ is the first material that combines highly efficient quantum cutting with absorption that is sufficiently strong and broad for practical solar applications.

Anion alloying can be used to reduce the energy gap (E_g) from ~3.05 eV (~405 nm) in $CsPbCl_3$ NCs to ~2.39 eV (~518 nm) in $CsPbBr_3$ NCs,[28−33] enabling the absorption of a much greater fraction of the solar spectrum. In principle, however, a fundamental energy-conservation threshold of $E_g > 2\times E_{f-f}$ must exist if quantum cutting is indeed responsible for Yb^{3+} PL sensitization in Yb^{3+}:$CsPb(Cl_{1-x}Br_x)_3$ NCs. From near-infrared (NIR) PL data,[19] we expect this absorption threshold to occur at $E_{f-f} \approx 2.53$ eV (~490 nm), but to date there has been no systematic investigation of the relationship between quantum cutting and E_g in such NCs. Quantum-

Received: December 21, 2018
Revised: January 14, 2019
Published: January 29, 2019

DOI: 10.1021/acs.nanolett.8b05104
Nano Lett. 2019, 19, 1931−1937

cutting polycrystalline films of Yb^{3+}:$CsPb(Cl_{1-x}Br_x)_3$ with substantially larger grain volumes do indeed show much smaller PLQYs in Yb^{3+}:$CsPbBr_3$ than in wider-gap compositions,[33] but only large step sizes along the halide composition parameter (x) were examined. The ability to finely tune the Yb^{3+}:$CsPbX_3$ energy gap would be attractive for characterizing the specific energy-conservation threshold, and hence the quantum-cutting mechanism itself, and should also be useful for optimizing the performance of these materials for various applications. In principle, such tunability could be achieved by postsynthetic anion exchange; $CsPbCl_3$ NCs readily undergo anion exchange with several common halide reagents to form mixed-halide alloys,[28−32] but to date, all quantum-cutting Yb^{3+}:$CsPbCl_3$ and Yb^{3+}:$CsPb(Cl_{1-x}Br_x)_3$ NCs[17,19,22] and polycrystalline films[19] have been prepared by direct synthesis only. Anion exchange has not yet been reported in any quantum-cutting perovskites. It is unclear whether anion exchange will retain the charge-neutral defect clusters thought to be integral to the Yb^{3+}:$CsPb(Cl_{1-x}Br_x)_3$ quantum-cutting mechanism[19] or whether such defects (or even the Yb^{3+} impurities themselves) may be passivated, dissociated, or extruded from the lattice during anion exchange, thereby sacrificing the high PLQYs.

Here we report a systematic investigation of the effects of $Cl^- \rightarrow Br^-$ anion exchange on the spectroscopic properties of Yb^{3+}:$CsPbX_3$ NCs. We find that it is possible to retain the high PLQYs of Yb^{3+}:$CsPbCl_3$ NCs ($E_g \approx 3.06$ eV, ~405 nm) during anion exchange while narrowing E_g to ~2.53 eV (~490 nm). For E_g below ~2.53 eV, the Yb^{3+} PLQY drops rapidly, demonstrating the anticipated energy threshold for quantum cutting. We further observe the sensitivity of the Yb^{3+} PLQY to the presence of water in the anion-exchange reaction, either from air or deliberately introduced into an otherwise dry reaction. Whereas the NC absorption spectra show no apparent sensitivity to residual water under our reaction conditions, the Yb^{3+} PL is substantially diminished (by as much as 40%) when anion exchange is performed in the presence of water.

Figure 1A shows TEM images of a representative sample of 7.7% Yb^{3+}:$CsPbCl_3$ NCs with average NC edge lengths of 14.1 ± 3.8 nm. The absorption and PL characteristics of $CsPbCl_3$ NCs are size-independent in this regime, and recent studies of Yb^{3+}:$CsPbCl_3$ polycrystalline thin films have demonstrated that quantum cutting is also largely unaffected by grain size.[19] Figure 1B shows TEM images of the same sample from Figure 1A after anion exchange to Yb^{3+}:$CsPbBr_3$ using trimethylsilyl bromide (TMS-Br) under dry, anaerobic conditions. The average NC size is now 14.8 ± 3.7 nm. A small degree of NC growth is to be expected due to the increase in lattice parameter, and some NCs appear to have fused together during the anion-exchange reaction. Figure 1C presents X-ray diffraction (XRD) patterns for the Yb^{3+}:$CsPbCl_3$ and Yb^{3+}:$CsPbBr_3$ NCs along with reference peaks for the respective compositions. The experimental diffraction pattern obtained after anion exchange matches the anticipated orthorhombic $CsPbBr_3$ diffraction. No crystalline impurities are observed in either composition. Combined, these data illustrate the successful conversion of $CsPbCl_3$ NCs into $CsPbBr_3$ NCs via anion exchange.

Figure 2A plots absorption spectra collected in situ during a representative NC anion-exchange reaction. Figure 2B plots in situ PL spectra for the same reaction. For this data set, the NCs were excited at 375 nm using a constant per-NC excitation rate

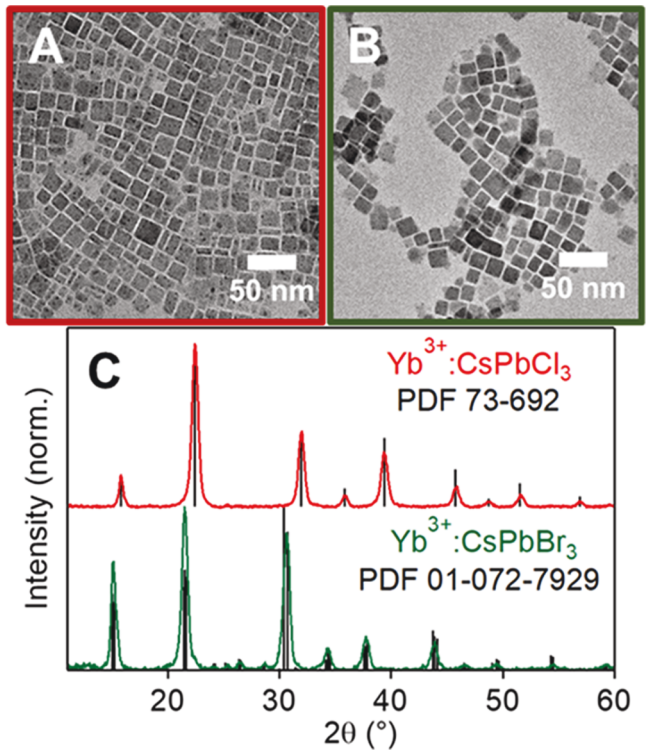

Figure 1. TEM images of 7.7% Yb^{3+}:$CsPbCl_3$ NCs collected (A) before and (B) after anaerobic anion exchange with TMS-Br in dry hexane, which converts Yb^{3+}:$CsPbCl_3$ NCs into Yb^{3+}:$CsPbBr_3$ NCs. (C) Representative XRD data for the same NCs from panel A. Reference diffraction patterns are included for comparison, confirming essentially complete anion exchange.

of 370 s^{-1}, with excitation powers adjusted during the course of the reaction according to the evolving optical density at 375 nm. The final absorption and PL spectra in this series exhibit the energy gap of $CsPbBr_3$, consistent with essentially complete anion exchange from Cl^- to Br^-. These data show that Yb^{3+} emission is still sensitized by NC photoexcitation, even in the final Yb^{3+}:$CsPbBr_3$ NCs, but this PL is substantially weaker in Yb^{3+}:$CsPbBr_3$ NCs than in Yb^{3+}:$CsPbCl_3$ or Yb^{3+}:$CsPb(Cl_{1-x}Br_x)_3$ NCs. Figure 2C summarizes these data by plotting the Yb^{3+} PL intensity versus the exciton PL wavelength from the data in Figure 2B. The PLQY of these specific Yb^{3+}:$CsPbCl_3$ NCs was ~114% before initiating the anion-exchange reaction. This plot shows that the Yb^{3+} PLQY remains above 100% until the first exciton shifts to below ~490 nm, at which point the Yb^{3+} PLQY drops rapidly with decreasing E_g. The narrowest energy gap where the full PLQY of the starting Yb^{3+}:$CsPbCl_3$ NCs corresponds to $x \approx 0.75$ in Yb^{3+}:$CsPb(Cl_{1-x}Br_x)_3$ NCs. Similar data have been obtained for many analogous samples, independent of PLQY (vide infra), consistent with this trend being intrinsic to the quantum-cutting mechanism itself. Overall, these data demonstrate the ability to finely tune E_g in quantum-cutting Yb^{3+}:$CsPb(Cl_{1-x}Br_x)_3$ NCs using anion exchange. Moreover, these results indicate that the quantum-cutting mechanism active in these materials remains effective despite the extensive lattice transformation that occurs during anion exchange.

The data in Figure 2C provide strong evidence of a discrete threshold energy for quantum cutting in these materials. The Yb^{3+} PL spectrum at low temperature shows its highest-energy feature at 1.267 eV (979 nm).[19] This feature is likely the first

DOI: 10.1021/acs.nanolett.8b05104
Nano Lett. 2019, 19, 1931−1937

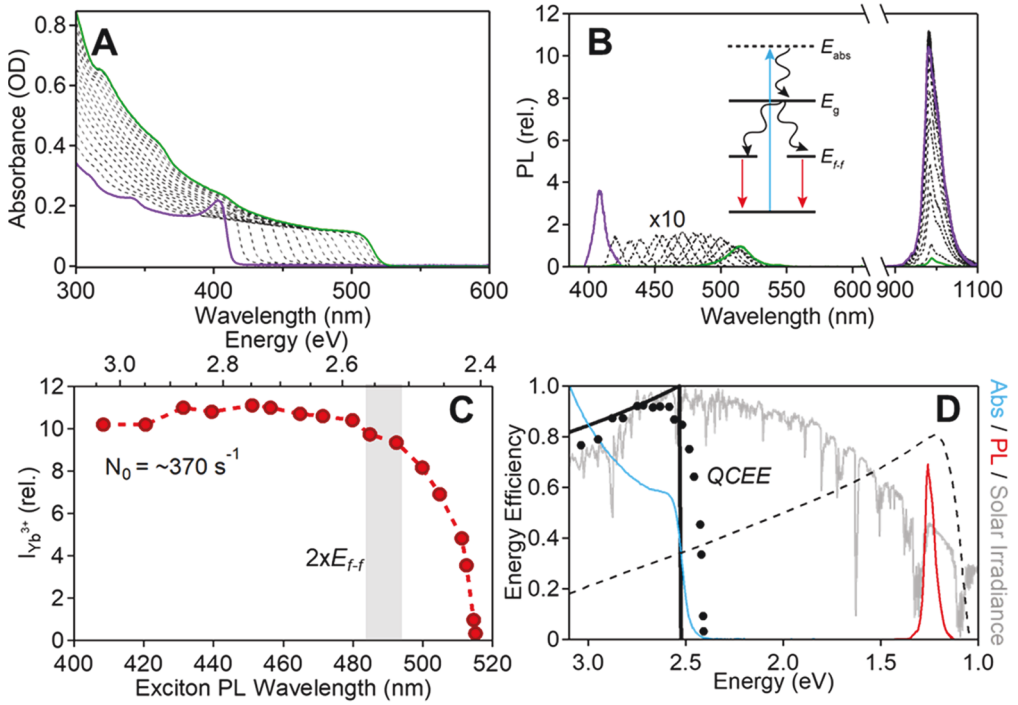

Figure 2. (A) Absorption spectra of 7.7% Yb^{3+}:$CsPb(Cl_{1-x}Br_x)_3$ NCs monitored in situ during anion exchange from Yb^{3+}:$CsPbCl_3$ (purple) to Yb^{3+}:$CsPbBr_3$ (green) using TMS-Br. (B) PL spectra collected in situ during the same reaction as in panel A. PL spectra were measured using 375 nm excitation at a constant NC excitation rate of ~370 s^{-1}. Absorption and PL spectra were recorded every ~14 min following the addition of TMS-Br. (C) Plot of the Yb^{3+} $^2F_{5/2} \rightarrow {}^2F_{7/2}$ PL intensity versus the exciton PL wavelength from the spectra in panel B. The gray shaded area marks approximately twice the Yb^{3+}($^2F_{7/2} \rightarrow {}^2F_{5/2}$) absorption onset ($2\times E_{f-f}$) estimated from the PL spectra, that is, the anticipated energy threshold for quantum cutting in these materials below which energy conservation cannot be maintained. (D) Data from panel C, replotted as quantum-cutting energy efficiency (QCEE, eq 1) versus E_{abs} (black circles), and eq 1 plotted for band-gap-optimized Yb^{3+}:$CsPb(Cl_{1-x}Br_x)_3$ NCs ($x \approx 0.75$, solid black curve) with an abrupt threshold. Both have been idealized to Φ_{max} = 200% for illustration. For comparison, the energy-conversion efficiency of a typical c-Si photovoltaic cell (dashed black), the AM1.5 solar spectral irradiance (gray), and the absorption (blue) and PL spectra (red) of the Yb^{3+}:$CsPb(Cl_{1-x}Br_x)_3$ NCs are also plotted. The inset in panel B illustrates the quantum-cutting process, including the thermalization loss when $E_{abs} > E_g \approx 2\times E_{f-f}$, such as in band-gap-optimized Yb^{3+}:$CsPb(Cl_{1-x}Br_x)_3$ NCs.

electronic origin within the crystal-field split $^2F_{5/2}$ multiplet, meaning it defines the low-temperature Yb^{3+}(f–f) absorption threshold as well. From the low-temperature origin, an energy threshold of $2\times E_{f-f}$ = 2.534 eV (489 nm) is thus anticipated, indicated by the gray vertical bar in Figure 2C. At room temperature, vibronic hot bands broaden the f–f absorption spectrum slightly to lower energy, and this threshold is expected to shift correspondingly. From Figure 2C, the Yb^{3+} PL intensity indeed drops precisely when the excitonic PL energy crosses $2\times E_{f-f}$.

The above results show that quantum cutting in Yb^{3+}:$CsPb(Cl_{1-x}Br_x)_3$ NCs has a very high intrinsic energy efficiency; that is, no step in the quantum-cutting mechanism introduces any substantial thermalization losses. This high energy efficiency is consistent with our recent proposal that quantum cutting in these materials proceeds via a shallow trap state residing just a few tens of millielectronvolts below the first exciton because the participation of a deeper trap state would result in PLQY losses that begin higher above $2\times E_{f-f}$ than observed in Figure 2C. To highlight this energy efficiency, the data from Figure 2C are replotted in Figure 2D in terms of the quantum-cutting energy efficiency (QCEE), as defined by eq 1. These data are compared with the numerical results from eq 1 in the limit of zero thermalization, that is, for an idealized PLQY of Φ = 200% above threshold and 0% below threshold and with a quantum-cutting threshold energy of $2\times E_{f-f}$. Φ for the experimental data has also been idealized to 200% at its maximum value for the purposes of comparison; experimental data from a nearly ideal sample (Φ ~ 200%) are shown in Figure S8 of the Supporting Information (SI). For the idealized curve, the QCEE begins at ~82% for 3.06 eV band-edge absorption in Yb^{3+}:$CsPbCl_3$ NCs (and also for 3.06 eV absorption in band-gap-optimized Yb^{3+}:$CsPb(Cl_{1-x}Br_x)_3$ NCs), and it approaches 100% as E_{abs} approaches $2\times E_{f-f}$, below which it drops rapidly to 0%. The experimental data follow this trend closely, except the drop-off is not as abrupt. Figure 2D also compares these QCEE plots with the energy-conversion efficiency curve of a high-performance c-Si photovoltaic cell. The latter has a value of only ~20% at 3.06 eV that increases to only ~35% at $2\times E_{f-f}$. These low energy-conversion efficiencies reflect the narrow E_g of Si and hence the large thermalization losses in Si photovoltaics when converting blue photons. A QCEE of 100% in this region would allow thermalization losses normally associated with above-band-gap photoexcitation to be eliminated entirely and instead replaced by the emission of an additional photon. As illustrated in Figure 2D, the Yb^{3+} emission from Yb^{3+}:$CsPb(Cl_{1-x}Br_x)_3$ NCs is very well aligned with the peak energy-conversion efficiency of c-Si photovoltaics. The high QCEEs of these Yb^{3+}:$CsPb(Cl_{1-x}Br_x)_3$ NCs thus motivate their use for eliminating thermalization losses in Si-based solar technologies.

$$\mathrm{QCEE} = \frac{E_{PL}}{E_{abs}}\Phi \approx \frac{1.267\ \mathrm{eV}}{E_{abs}}\Phi \qquad (1)$$

DOI: 10.1021/acs.nanolett.8b05104
Nano Lett. 2019, 19, 1931−1937

In addition to high QCEEs, the *curvature* of the data in Figure 2C appears to be an intrinsic characteristic of this material system. Very similar curvature has been obtained in many analogous anion-exchange experiments for samples with many PLQYs, reaching as high as ~200% (see the SI). Two potential sources of this curvature could be (i) loss of Yb^{3+} during anion exchange and (ii) PL power saturation.[19] The former possibility is ruled out by inductively coupled plasma atomic emission spectroscopy (ICP-AES) measurements showing that the Yb^{3+} content remains unchanged over the entire anion-exchange composition series, bolstered by the observation that converting product Yb^{3+}:$CsPbBr_3$ NCs back to Yb^{3+}:$CsPbCl_3$ NCs via anion exchange using oleylammonium chloride returns the Yb^{3+} PLQY to within ~20% of its original value, that is, well above 100% (see the SI). The latter possibility is ruled out by performing the experiment at a constant excitation rate (Figure 2). When similar measurements are instead performed with a constant excitation source (fixed excitation wavelength and power density, e.g., Figure 3A), then saturation also adds slightly to the decrease in PLQY with decreasing E_g (see the SI) because anion exchange leads to increased NC excitation rates under these conditions. Instead of these two scenarios, it appears likely that the curvature seen in Figure 2C is intrinsic to the material and reflects changes in the energy matching between the energy donor (shallow trap) and energy acceptor ($2\times E_{f-f}$) states involved in quantum cutting. Such energy matching is required for energy conservation and hence contributes to the nonradiative energy-transfer rate, as summarized by Fermi's golden rule (eq 2, where R_{if} is the energy-transfer rate, M_{if} is the electronic-coupling matrix element for the donor−acceptor interaction, and ρ_f is the density of acceptor states at the energy of the donor state, summed over donor energies). Our previous work has shown that trivalent-cation-doped $CsPbCl_3$ NCs have a broad trap-state PL with a peak maximum ~40 meV below the exciton PL,[19] indicating a multitude of viable donor energies and associated probabilities. This breadth, in conjunction with thermal broadening of the Yb^{3+}(f−f) absorption, causes the drop in R_{if} to be broadened in energy somewhat during the transition from the quantum-cutting ($E_g > 2\times E_{f-f}$) regime to the non-quantum-cutting regime ($E_g < 2\times E_{f-f}$) with anion exchange (Figure 2C).

$$R_{if} = \frac{2\pi}{\hbar}|M_{if}|^2\rho_f \tag{2}$$

In the course of these anion-exchange measurements, we also noticed variations in the specific curves obtained under nominally similar reaction conditions, and we identified the presence of trace water as an important factor. For illustration, Figure 3A plots the Yb^{3+} PL intensity versus the exciton PL wavelength for reactions performed rigorously anaerobically (as in Figure 2) and aerobically. The Yb^{3+} PL of the aerobic anion-exchange reaction decreases already during the initial anion-exchange steps and remains ~20% lower than the reference anaerobic data set until the quantum-cutting threshold of ~489 nm is reached, beyond which the Yb^{3+} PL intensities in both data sets drop rapidly. Similarly, Figure 3B plots excitonic PL intensities versus exciton PL wavelength collected during the same reactions, as shown in Figure 3A. Under anaerobic conditions, the excitonic PL intensity remains nearly constant throughout the entire anion-exchange reaction. When the reaction is performed aerobically, however, the exciton PL intensity increases by approximately an order of magnitude upon conversion from Yb^{3+}:$CsPbCl_3$ to Yb^{3+}:$CsPbBr_3$. For both reaction conditions, TMS-Br and benzoyl bromide anion-exchange reagents yield similar results. We note that both anion-exchange reagents react with water to form HBr, which may therefore be generated in situ under experimental conditions involving water and may be relevant to the observed influence of water.

A major difference between reactions performed with and without water present is their kinetics. Figure 4 plots absorption spectra of Yb^{3+}:$CsPbCl_3$ NCs collected before and after anion exchange using TMS-Br for reactions performed under three different conditions: anaerobically in dry hexane, aerobically in aerated hexane, and anaerobically with water added to dry hexane (Figures 4A−C, respectively). Although all three data sets appear essentially identical, they arose from reactions with very different kinetics. Figure 4D plots the time evolution of the absorbance at 375 nm collected during each of these three anion-exchange reactions. Whereas the aerobic reaction was complete within 15 min, the anaerobic reaction took over 4 h to reach completion. The entire kinetic trace for the anaerobic reaction is included in the inset of Figure 4D. Figure 4E summarizes the Yb^{3+} PL intensities measured during the same anion-exchange reactions. For the anaerobic reaction, the Yb^{3+} PL intensity remained constant until the energy gap reached ~489 nm, as in Figure 2C. Adding

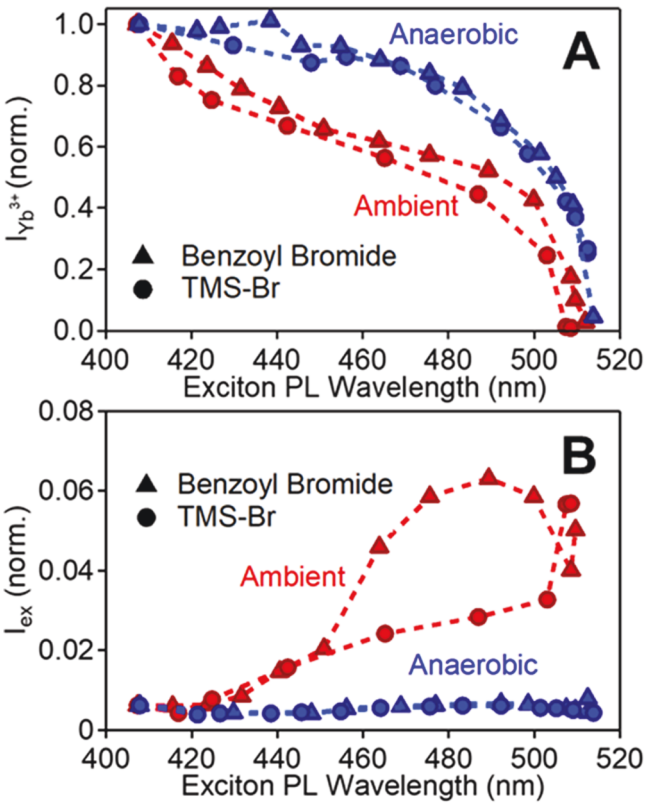

Figure 3. Relative (A) Yb^{3+} NIR (985 nm) and (B) excitonic PL intensities plotted versus excitonic PL wavelength, collected during $Cl^- \rightarrow Br^-$ anion exchange of 5.5% Yb^{3+}:$CsPbCl_3$ NCs using either TMS-Br or benzoyl bromide. PL intensities were collected using constant excitation power at 375 nm. Data were subsequently corrected for the changing absorbance at 375 nm but not for changes in PL saturation. All intensities are normalized to the Yb^{3+} PL intensity of the starting Yb^{3+}:$CsPbCl_3$ NCs. Note the different *y*-axis scales.

DOI: 10.1021/acs.nanolett.8b05104
Nano Lett. 2019, 19, 1931−1937

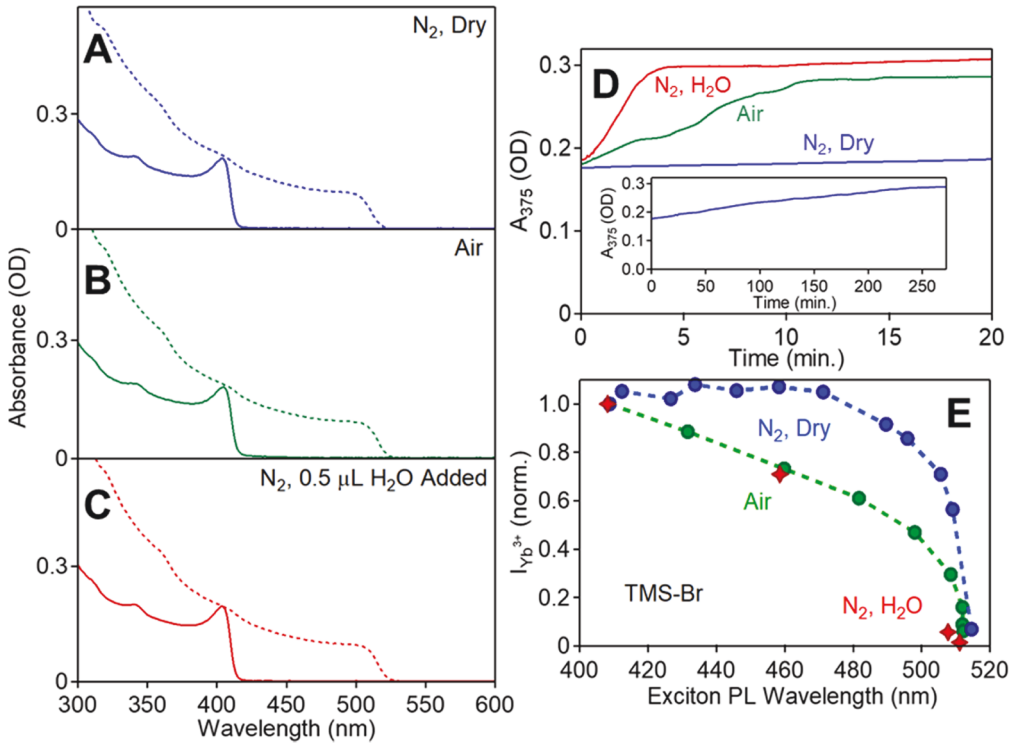

Figure 4. Absorption spectra of 5.5% Yb^{3+}:$CsPbCl_3$ NCs collected before (solid lines) and after (dotted lines) anion exchange using TMS-Br under three different reaction conditions: (A) anaerobic in dry hexane, (B) aerobic in hexane, and (C) anaerobic in dry hexane with added water (0.5 μL of H_2O added to 3 mL of dry hexane). (D) Kinetic traces monitoring the NC absorbance at 375 nm (A_{375}) following injection of TMS-Br under the three reaction conditions from panels A–C. Inset: Entire kinetic trace for the anaerobic anion-exchange reaction in dry hexane. (E) Intensity of Yb^{3+} PL at 985 nm plotted versus exciton PL wavelength for the same three anion-exchange reactions, reacting 5.5% Yb^{3+}:$CsPbCl_3$ NCs with TMS-Br anaerobically in dry hexane (blue), aerobically (green), and anaerobically with 0.2 μL of water added to 3 mL of dry hexane (red).

water to the reaction or aerating the solution both caused a decrease in Yb^{3+} PL intensity in earlier stages of the anion-exchange reaction. For example, when the exciton PL was at 475 nm, the aerobic reaction showed Yb^{3+} PL intensities that were ~40% smaller than those of the anaerobic, dry reaction.

One conceivable cause for the disparity between PL intensities obtained for anaerobic versus aerobic (hydrated) anion exchange could be a difference in the NCs themselves that results from the introduction of water, for example, through extensive Ostwald ripening, oriented attachment, or NC dissolution. To test for such differences, the same reactions were probed by TEM, for both undoped and Yb^{3+}-doped NCs. Figure 5 shows TEM images of undoped $CsPbCl_3$ and 4.1% Yb^{3+}-doped $CsPbCl_3$ NCs collected before and after anion exchange under the anaerobic and aerobic reaction conditions described in Figure 4. Whether the reaction is performed anaerobically (slowly) or aerobically (rapidly), the NCs appear to grow slightly and maintain their cubic morphologies. Although some larger crystallites are observed after anion exchange that appear to arise from oriented attachment during reaction, the formation of such morphologies is independent of Yb^{3+} doping. Figure 5D,H plots size-distribution histograms for these reactions with the undoped and doped NCs, respectively. The undoped NCs started with an edge length of 12.8 ± 3.3 nm, and this dimension grew to 13.7 ± 4.0 nm when anion exchange was performed aerobically compared with 14.2 ± 5.7 nm when the reaction was performed anaerobically. The Yb^{3+}-doped NCs had a starting edge length of 11.8 ± 2.3 nm that grew to 14.7 ± 4.1 nm under aerobic reaction conditions compared with 14.4 ± 4.3 nm under anaerobic conditions. These data show that the large increase in reaction rate and the substantial drop in Yb^{3+} PLQY observed when using aerobic reaction conditions are not accompanied by any detectable change in NC size or morphology. The effect of water on Yb^{3+} PL intensities during anion exchange thus appears to have a microscopic origin.

We hypothesize that the presence of water may cause Yb^{3+} to be extruded from the NCs during the anion-exchange reaction, thereby eliminating the charge-neutral lattice defect clusters believed to be responsible for quantum cutting in these materials.[19] Such extraction could be driven by the coordination of Yb^{3+} by water, given the high oxophilicity of Yb^{3+}. We have not observed any particularly strong sensitivity of Yb^{3+}:$CsPb(Cl_{1-x}Br_x)_3$ NCs to water under ambient storage conditions, which suggests that the lattice reorganization during anion exchange facilitates this deactivation of Yb^{3+} PL. These results are particularly striking in light of the opposite trend observed in the excitonic PL intensities, which *increase* when the reaction is performed in the presence of water (Figure 3B and the SI). Although the detailed microscopic mechanism of Yb^{3+} PL deactivation is still not entirely clear, these results highlight the need for dry solvents and atmosphere when tuning E_g in quantum-cutting Yb^{3+}:$CsPb(Cl_{1-x}Br_x)_3$ NCs via anion exchange.

In summary, we have demonstrated the use of anion-exchange chemistries to tune the energy gaps of Yb^{3+}:$CsPb(Cl_{1-x}Br_x)_3$ NCs continuously from $0 \leq x \leq \sim 1$. Quantum cutting is retained for x values as large as ~0.75, corresponding to ~2.53 eV (~489 nm). At larger x, a steep drop in PLQY is observed that is attributed to crossing an energy-conservation

DOI: 10.1021/acs.nanolett.8b05104
Nano Lett. 2019, 19, 1931–1937

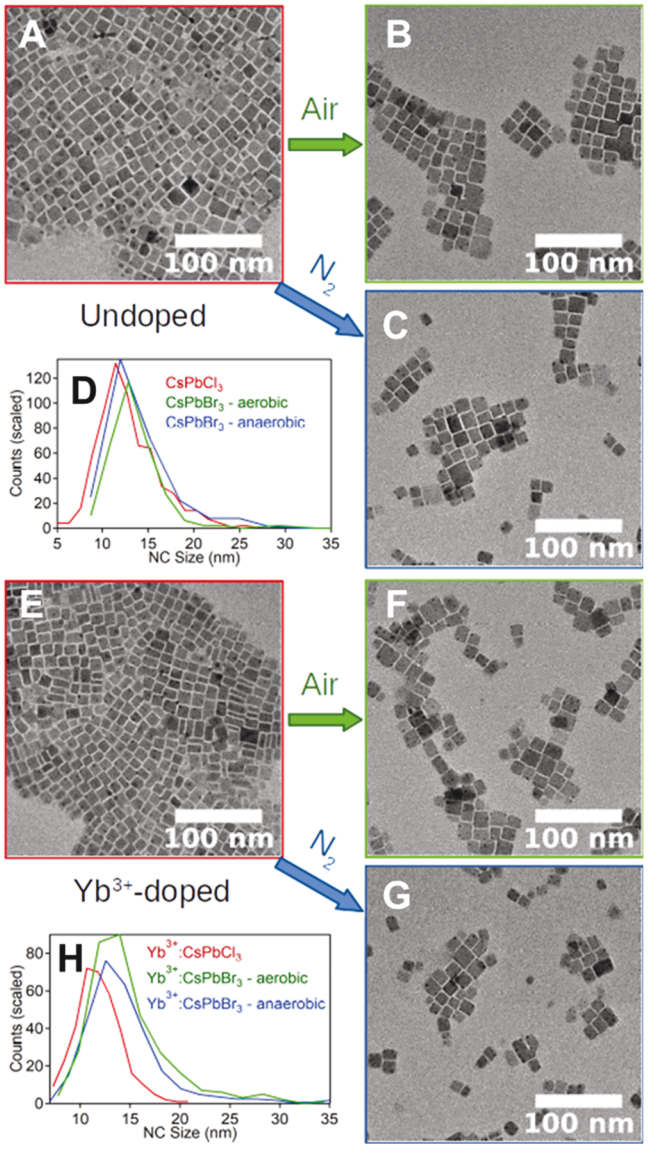

Figure 5. TEM images and size distributions of (A–D) undoped $CsPbCl_3$ NCs and (E–H) 4.1% Yb^{3+}:$CsPbCl_3$ NCs collected before (A,E) and after (B,C,F,G) anion-exchange conversion to $CsPbBr_3$ and Yb^{3+}:$CsPbBr_3$ NCs using TMS-Br. Anion-exchange reactions were performed either aerobically after aerating dry hexane (green, rapid reaction) or anaerobically (blue, slow reaction), as indicated in the figure and described by Figure 4.

threshold. This threshold is a signature of the quantum-cutting mechanism. These results thus demonstrate that it is possible to tune E_g of quantum-cutting perovskite NCs over a reasonably large range to optimize these materials for solar- or other spectral-conversion technologies without the loss of PLQY. For example, for solar spectral downconversion applications involving Si, Yb^{3+}:$CsPbCl_3$ NCs absorb only ~3.3% of the solar photons above the Si absorption threshold of 1.1 eV (~2.1% of all AM1.5 solar photons), but Yb^{3+}:$CsPb(Cl_{0.25}Br_{0.75})_3$ NCs with the same PLQY can absorb ~13.2% of the solar photons absorbed by Si (~8.5% of all AM1.5 solar photons). The absorption of these blue photons and reemission of that energy by Yb^{3+} with nearly perfect quantum-cutting energy efficiency may allow a sizable reduction in the thermalization losses of Si photovoltaics.

In addition to demonstrating the retention of high PLQYs in quantum-cutting perovskite NCs during postsynthetic energy-gap tuning via anion exchange, the experiments here also demonstrate that anion exchange *does* diminish the PLQY substantially if the reaction is performed in the presence of water, even when E_g is still well above the quantum-cutting threshold. Water accelerates the anion-exchange reaction tremendously, independent of Yb^{3+}, but there is no detectable dependence of the NC morphology or average size on this reaction rate, suggesting that the loss of Yb^{3+} PLQY has a microscopic origin. In fact, the excitonic PLQY in undoped NCs actually increases when the anion-exchange reaction is performed in the presence of water, showing that water's influence is specific to Yb^{3+}. The reduction of Yb^{3+} PLQY during anion-exchange reactions performed in the presence of water is tentatively attributed to loss of Yb^{3+} from the internal NC volume, aided by its high oxophilicity. Overall, the results presented here provide new fundamental insight into the unique quantum-cutting process displayed by these NCs and also offer valuable practical guidance for tuning the spectral characteristics of such NCs to optimize their performance in future solar and photonics applications.

■ ASSOCIATED CONTENT

Supporting Information

The Supporting Information is available free of charge on the ACS Publications website at DOI: 10.1021/acs.nanolett.8b05104.

Experimental details, additional sample characterization, and spectroscopic data (PDF)

■ AUTHOR INFORMATION

Corresponding Author

*E-mail: gamelin@chem.washington.edu.

ORCID

Tyler J. Milstein: 0000-0002-1517-2222
Kyle T. Kluherz: 0000-0002-7986-5167
Daniel M. Kroupa: 0000-0002-2788-3670
Christian S. Erickson: 0000-0001-7888-0034
James J. De Yoreo: 0000-0002-9194-6699
Daniel R. Gamelin: 0000-0003-2888-9916

Notes

The authors declare no competing financial interest.

■ ACKNOWLEDGMENTS

This research was supported by the National Science Foundation (NSF) through the UW Molecular Engineering Materials Center, a Materials Research Science and Engineering Center (DMR-1719797). Additional support from DMR-1807394 (to D.R.G.) and the Washington Research Foundation (to D.M.K.) is gratefully acknowledged. Part of this work was conducted at the UW Molecular Analysis Facility, a National Nanotechnology Coordinated Infrastructure site supported in part by the NSF (ECC-1542101), the University of Washington, the Molecular Engineering and Sciences Institute, the Clean Energy Institute, and the National Institutes of Health. Dr. Matthew Crane is acknowledged for assistance with the solar-flux calculations.

DOI: 10.1021/acs.nanolett.8b05104
Nano Lett. 2019, 19, 1931–1937

REFERENCES

(1) Protesescu, L.; Yakunin, S.; Bodnarchuk, M. I.; Krieg, F.; Caputo, R.; Hendon, C. H.; Yang, R. X.; Walsh, A.; Kovalenko, M. V. *Nano Lett.* **2015**, *15*, 3692−3696.
(2) ten Brinck, S.; Infante, I. *ACS Energy Lett.* **2016**, *1*, 1266−1272.
(3) Akkerman, Q. A.; Rainò, G.; Kovalenko, M. V.; Manna, L. *Nat. Mater.* **2018**, *17*, 394−405.
(4) Yakunin, S.; Protesescu, L.; Krieg, F.; Bodnarchuk, M. I.; Nedelcu, G.; Humer, M.; De Luca, G.; Fiebig, M.; Heiss, W.; Kovalenko, M. V. *Nat. Commun.* **2015**, *6*, 8056.
(5) Ramasamy, P.; Lim, D.-H.; Kim, B.; Lee, S.-H.; Lee, M.-S.; Lee, J.-S. *Chem. Commun.* **2016**, *52*, 2067−2070.
(6) Swarnkar, A.; Marshall, A. R.; Sanehira, E. M.; Chernomordik, B. D.; Moore, D. T.; Christians, J. A.; Chakrabarti, T.; Luther, J. M. *Science* **2016**, *354*, 92.
(7) Sanehira, E. M.; Marshall, A. R.; Christians, J. A.; Harvey, S. P.; Ciesielski, P. N.; Wheeler, L. M.; Schulz, P.; Lin, L. Y.; Beard, M. C.; Luther, J. M. *Sci. Adv.* **2017**, *3*, eaao4204.
(8) Swarnkar, A.; Ravi, V. K.; Nag, A. *ACS Energy Lett.* **2017**, *2*, 1089−1098.
(9) van der Stam, W.; Geuchies, J. J.; Altantzis, T.; van den Bos, K. H. W.; Meeldijk, J. D.; Van Aert, S.; Bals, S.; Vanmaekelbergh, D.; de Mello Donega, C. *J. Am. Chem. Soc.* **2017**, *139*, 4087−4097.
(10) Yao, J.-S.; Ge, J.; Han, B.-N.; Wang, K.-H.; Yao, H.-B.; Yu, H.-L.; Li, J.-H.; Zhu, B.-S.; Song, J.-Z.; Chen, C.; Zhang, Q.; Zeng, H.-B.; Luo, Y.; Yu, S.-H. *J. Am. Chem. Soc.* **2018**, *140*, 3626−3634.
(11) Parobek, D.; Roman, B. J.; Dong, Y.; Jin, H.; Lee, E.; Sheldon, M.; Son, D. H. *Nano Lett.* **2016**, *16*, 7376−7380.
(12) Liu, W.; Lin, Q.; Li, H.; Wu, K.; Robel, I.; Pietryga, J. M.; Klimov, V. I. *J. Am. Chem. Soc.* **2016**, *138*, 14954−14961.
(13) Lin, C. C.; Xu, K. Y.; Wang, D.; Meijerink, A. *Sci. Rep.* **2017**, *7*, 45906.
(14) Yuan, X.; Ji, S.; De Siena, M. C.; Fei, L.; Zhao, Z.; Wang, Y.; Li, H.; Zhao, J.; Gamelin, D. R. *Chem. Mater.* **2017**, *29*, 8003−8011.
(15) Xu, K.; Lin, C. C.; Xie, X.; Meijerink, A. *Chem. Mater.* **2017**, *29*, 4265−4272.
(16) Mir, W. J.; Mahor, Y.; Lohar, A.; Jagadeeswararao, M.; Das, S.; Mahamuni, S.; Nag, A. *Chem. Mater.* **2018**, *30*, 8170−8178.
(17) Zhou, D.; Liu, D.; Pan, G.; Chen, X.; Li, D.; Xu, W.; Bai, X.; Song, H. *Adv. Mater.* **2017**, *29*, 1704149.
(18) Pan, G.; Bai, X.; Yang, D.; Chen, X.; Jing, P.; Qu, S.; Zhang, L.; Zhou, D.; Zhu, J.; Xu, W.; Dong, B.; Song, H. *Nano Lett.* **2017**, *17*, 8005−8011.
(19) Milstein, T. J.; Kroupa, D. M.; Gamelin, D. R. *Nano Lett.* **2018**, *18*, 3792−3799.
(20) van der Ende, B. M.; Aarts, L.; Meijerink, A. *Adv. Mater.* **2009**, *21*, 3073−3077.
(21) van der Ende, B. M.; Aarts, L.; Meijerink, A. *Phys. Chem. Chem. Phys.* **2009**, *11*, 11081−11095.
(22) Luo, X.; Ding, T.; Liu, X.; Liu, Y.; Wu, K. *Nano Lett.* **2019**, *19*, 338−341.
(23) Meijer, J.-M.; Aarts, L.; van der Ende, B. M.; Vlugt, T. J. H.; Meijerink, A. *Phys. Rev. B: Condens. Matter Mater. Phys.* **2010**, *81*, 035107.
(24) Creutz, S. E.; Fainblat, R.; Kim, Y.; De Siena, M. C.; Gamelin, D. R. *J. Am. Chem. Soc.* **2017**, *139*, 11814−11824.
(25) Shao, W.; Lim, C.-K.; Li, Q.; Swihart, M. T.; Prasad, P. N. *Nano Lett.* **2018**, *18*, 4922−4926.
(26) Wang, Z.; Meijerink, A. J. *J. Phys. Chem. Lett.* **2018**, *9*, 1522−1526.
(27) Rufino Souza, A. K.; Langaro, A. P.; Silva, J. R.; Costa, F. B.; Yukimitu, K.; Silos Moraes, J. C.; Antonio de Oliveira Nunes, L.; Humberto da Cunha Andrade, L.; Lima, S. M. *J. Alloys Compd.* **2019**, *781*, 1119−1126.
(28) Nedelcu, G.; Protesescu, L.; Yakunin, S.; Bodnarchuk, M. I.; Grotevent, M. J.; Kovalenko, M. V. *Nano Lett.* **2015**, *15*, 5635−5640.
(29) Akkerman, Q. A.; D'Innocenzo, V.; Accornero, S.; Scarpellini, A.; Petrozza, A.; Prato, M.; Manna, L. *J. Am. Chem. Soc.* **2015**, *137*, 10276−10281.
(30) Parobek, D.; Dong, Y.; Qiao, T.; Rossi, D.; Son, D. H. *J. Am. Chem. Soc.* **2017**, *139*, 4358−4361.
(31) Imran, M.; Caligiuri, V.; Wang, M.; Goldoni, L.; Prato, M.; Krahne, R.; De Trizio, L.; Manna, L. *J. Am. Chem. Soc.* **2018**, *140*, 2656−2664.
(32) Creutz, S. E.; Crites, E. N.; De Siena, M. C.; Gamelin, D. R. *Chem. Mater.* **2018**, *30*, 4887−4891.
(33) Kroupa, D. M.; Roh, J. Y.; Milstein, T. J.; Creutz, S. E.; Gamelin, D. R. *ACS Energy Lett.* **2018**, *3*, 2390−2395.

DOI: 10.1021/acs.nanolett.8b05104
Nano Lett. 2019, 19, 1931−1937